Quantitative Theory of Adsorptive Separation for the Electronic Sorting of Single-Walled Carbon Nanotubes
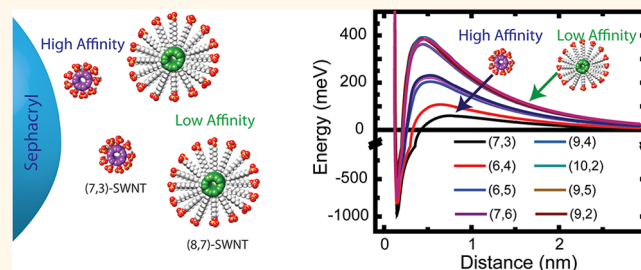
Rishabh M. Jain,[‡,§] Kevin Tvrdy,[†,§] Rebecca Han,[†] Zachary Ulissi,[†] and Michael S. Strano[†,*]

[†]Departments of Chemical Engineering and [‡]Materials Science Engineering, Massachusetts Institute of Technology, 77 Massachusetts Avenue, Cambridge, Massachusetts 02139, United States. [§]R. M. Jain and K. Tvrdy contributed equally to this work.

ABSTRACT Recently, several important advances in techniques for the separation of single-walled carbon nanotubes (SWNTs) by chiral index have been developed. These new methods allow for the separation of SWNTs through selective adsorption and desorption of different (*n,m*) chiral indices to and from a specific hydrogel. Our group has previously developed a kinetic model for the chiral elution order of separation; however, the underlying mechanism that allows for this separation remains unknown. In this work, we develop a quantitative theory that provides the first mechanistic insights for the separation order and binding kinetics of each SWNT chirality (*n,m*) based on the surfactant-induced, linear charge density, which we find ranges from 0.41 e$^-$/nm for (7,3) SWNTs in 17 mM sodium dodecyl sulfate (SDS) to 3.32 e$^-$/nm for (6,5) SWNTs in 105 mM SDS. Adsorption onto the hydrogel support is balanced by short-distance hard-surface and long-distance electrostatic repulsive SWNT/substrate forces, the latter of which we postulate is strongly dependent on surfactant concentration and ultimately leads to gel-based single-chirality semiconducting SWNT separation. These molecular-scale properties are derived using bulk-phase, forward adsorption rate constants for each SWNT chirality in accordance with our previously published model. The theory developed here quantitatively describes the experimental elution profiles of 15 unique SWNT chiralities as a function of anionic surfactant concentration between 17 and 105 mM, as well as phenomenological observations of the impact of varying preparatory conditions such as extent of ultrasonication and ultracentrifugation. We find that SWNT elution order and separation efficiency are primarily driven by the morphological change of SDS surfactant wrapping on the surface of the nanotube, mediated by SWNT chirality and the ionic strength of the surrounding medium. This work provides a foundational understanding for high-purity, preparative-scale separation of as-produced SWNT mixtures into isolated, single-chirality fractions.

KEYWORDS: single-walled carbon nanotube · mechanism · single chirality · separation · sodium dodecyl sulfate · Sephacryl gel

Single-walled carbon nanotubes (SWNTs) exhibit extraordinary mechanical, thermal, electronic, and optical properties that have found applications in biological sensing,[1,2] optoelectronics,[3−10] and materials development.[11−13] Recent developments by the groups of Kataura and Kappes enabling separation of preparative quantities of semiconducting SWNTs based on their chiral wrapping vector (*n,m*)[14−23] have furthered investigations into the effects of chiral inhomogeneity on photovoltaic[5,6,8,24] and biosensor[25] performance. Pioneered by the use of a commercially available amide-functionalized dextran hydropolymer (Sephacryl S200)[22] as a separation medium and the further discovery of single-surfactant (sodium dodecyl sulfate, SDS) interaction conditions that yield single-chirality separation,[26] we have quantitatively described gel-based SWNT separation as a second-order forward reaction with chirality-dependent kinetic rate constants.[27] However, the mechanism by which varying SDS concentration affects the selective adsorption/desorption of SWNT to Sephacryl, which ultimately enables separation of single-chirality SWNTs, remains unknown. The fundamental SWNT−SDS−Sephacryl interactions[22,26,27] need to be better understood in order to further advance single-chirality SWNT separation. Kataura and co-workers have recently provided qualitative demonstrations that temperature affects the chiralities that can be separated *via* a change in the SDS state;[28] more recently they proposed a qualitative model of how SDS morphology affects the relative affinity of metal *versus* semiconducting carbon nanotubes when separated

using a gel.[29] Additionally, Hennrich and co-workers offered an experimental description of the effects of pH and 1-dodecanol on gel-based SWNT separation.[30] Finally, work by Schapter and colleagues observed experimentally that SDS changes the resultant separation.[31] While these experimental demonstrations reveal the importance of SDS and SDS concentration, a specific description of the role that the surfactant plays for single-chirality semiconducting carbon nanotube separation is as yet unclear. In this work, we develop the first quantitative theory of this adsorptive separation, which describes the elution order, adsorption kinetics, and surfactant and ionic strength dependences observed experimentally. By relating phenotypical variables of SWNT separation under a single model, we demonstrate and provide novel insight into the molecular-scale interactions that control separation. We introduce a new parameter, $\xi_{n,m}$, defined as the chirality- and surfactant concentration-dependent effective charge density associated with SDS-wrapped SWNTs, which ultimately determines the efficiency, diameter range, and purity of single-chirality SWNT separation. This charge density is physically due to the incomplete cationic association of Na^+ with the SWNT association dodecylsulfate anion, a phenomenon demonstrated previously in SDS micelles.[32]

This work is distinguished from previous contributions that have been informative but largely qualitative.[28−31,33−35] Our group was the first to provide a quantitative analysis of the separation process, reporting the binding rate constants for semiconducting SWNTs with Sephacryl gel at 70 mM SDS concentration[27] and showing that the elution profiles and selectivity were well described by a second-order irreversible adsorption mechanism. However, the molecular-scale origin of these forward rate constants and their dependence on SWNT chirality remained unaddressed.[36] Here, we expand upon our previous forward binding rate model[27] to provide a molecular-scale picture of the separation procedure, as validated experimentally through perturbation of surfactant concentration. Furthermore, some of the experimental steps proposed to achieve SWNT separation, such as the need to expose bulk-synthesized SWNT materials to harsh ultrasonication for 20 h, lack a clear explanation. Understanding the role of these procedures and how they ultimately affect the resultant separation is important to further optimize this process.

Some insight into the relationship between surfactant and SWNT optical and physical properties has already been achieved.[22,37−42] Further, it has been previously demonstrated that surfactant-enabled colloidal suspensions of individualized SWNT retain a per-SWNT charge, which can be used to predict relative material stability.[43] The choice of optimal surfactant for SWNT separation has also been the subject of investigation, and of the many types screened, SDS was shown to be paramount in its ability to separate metallic from semiconducting SWNTs.[36]

In this article, we first outline the quantitative molecular-scale model, which empirically describes the surfactant-mediated binding of SWNT to Sephacryl gel. We then report observations made when perturbing the standard experimental procedure with regard to both the SWNT suspension and the surfactant medium and relate these observations to the model developed herein. The methods section describes the standard experimental procedure used to achieve monosurfactant single-chirality SWNT separation.[26,27] Understanding this separation process in a comprehensive way enables the engineered design of more efficient and specifically tailored SWNT separation procedures for broader application of SWNTs in semiconductor, biosensor, and other applications.

MODEL FORMULATION

To model the interaction involving the SDS-mediated adsorption and desorption of SWNTs to and from a Sephacryl binding site, it is important to consider the physical properties of all three materials involved in these events, depicted geometrically in Figure 1A. The
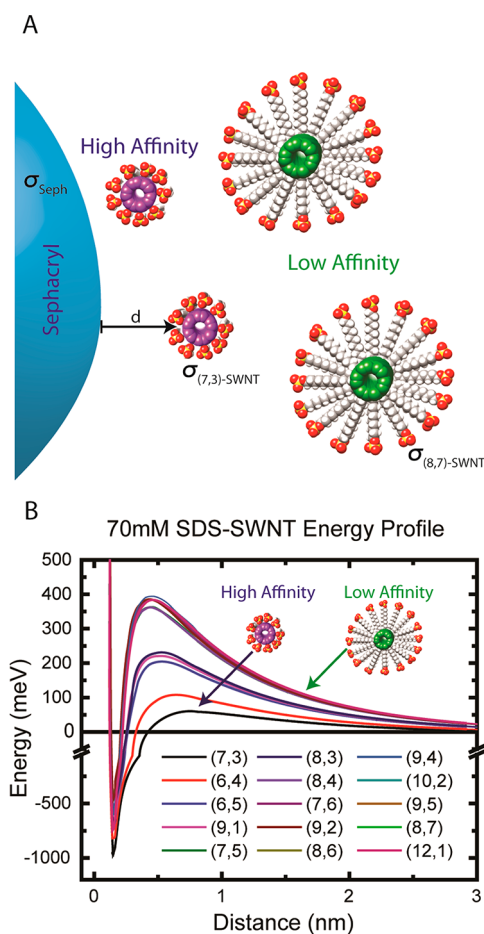

Figure 1. (A) Graphical representation of SDS-wrapped SWNT and the parameters that are important to its interaction with the gel, displayed here as a sphere. **(B)** Chirality-dependent energy profile as a function of SWNT−Sephacryl surface separation distance in the presence of 70 mM SDS.

binding of a semiconducting SWNT to a Sephacryl site can be generally described in terms of the total system energy $V(d)$ as a function of the distance between the Sephacryl and SWNT surfaces, d. Here, we estimate this energy as the sum of three unique distance-dependent contributions: van der Waals attractive ($V_{\text{van der Waals}}$), electrostatic repulsive ($V_{\text{electrostatic}}$), and hard-surface repulsive ($V_{\text{hard surface}}$) forces.

$$V(d) = V_{\text{van der Waals}}(d) - V_{\text{electrostatic}}(d) - V_{\text{hard sphere}}(d) \tag{1}$$

The attractive energy between SWNT and a Sephacryl binding site is modeled to first-order by the van der Waals interaction between an anisotropic planar surface and a SWNT of radius r_{SWNT}, as described previously by Rajter et al.[44] and utilized to describe the interactions of type-purified SWNTs with both quartz and polymer substrates.[45]

$$V_{\text{van der Waals}}(d) = \left[-\frac{\sqrt{2r_{\text{SWNT}}}}{24d^{3/2}}\left(\frac{3}{2}H_N\right)\left(\frac{1}{1+e^{\beta(d-d_0)}}\right) \right.$$
$$\left. -\frac{r_{\text{SWNT}}^2}{6(d+r_{\text{SWNT}})^3}\left(\frac{3}{2}H_F\right) \times \left(1 - \frac{1}{1+e^{\beta(d-d_0)}}\right) \right] / l \tag{2}$$

where H_N and H_F are the Hamaker coefficients in the near and far limit of SWNT–plane separation, respectively, and β and d_0 are blending terms accounting for the transition between short- and long-range interactions.[44]

Electrostatically, we assign a repulsive force which arises from the common anionic charge shared by the amide binding site on Sephacryl 200 and the SWNT.[43] The radially dependent interaction between a plane of uniform charge density (σ_{SEPH}) and a plane of uniform charge density wrapped into a cylinder (σ_{SWNT}) of radius r_{SWNT} and length l, both surrounded by a liquid with dielectric permittivity ε and Debye length κ, has been solved by Oshima et al.:[46]

$$V_{\text{Electrostatic}}(d) = \varepsilon\varepsilon_0\sqrt{\pi\kappa r_{\text{SWNT}}}\left(2\sqrt{2}\left(\frac{\sigma_{\text{SEPH}}}{\varepsilon\varepsilon_0\kappa}\right)\right.$$
$$\times \left(\frac{\sigma_{\text{SWNT}}}{\varepsilon\varepsilon_0\kappa}\frac{K_0(\kappa r_{\text{SWNT}})}{K_1(\kappa r_{\text{SWNT}})}\right)e^{-\kappa d} + \left(\frac{\sigma_{\text{SEPH}}}{\varepsilon\varepsilon_0\kappa}\right)^2 e^{-2\kappa d}$$
$$\left. + \left(\frac{\sigma_{\text{SWNT}}}{\varepsilon\varepsilon_0\kappa}\frac{K_0(\kappa r_{\text{SWNT}})}{K_1(\kappa r_{\text{SWNT}})}\right)^2 \times \sqrt{\frac{r_{\text{SWNT}}}{r_{\text{SWNT}}+d}}e^{-2\kappa d}\right) / l \tag{3}$$

where ε_0 is the vacuum permittivity and K_n is the modified Bessel function of the nth kind.

The assumption of an interaction with the amide group is not central to the theory developed here, as the system is equilibrated in SDS; thus it may be the case that ionized SDS molecules on the gel provide the repulsive force. This would be similar to the commonly implemented SDS-PAGE technique, where SDS is used in order to stabilize proteins against aggregation

through the introduction of a charged surfactant. This does not, however, explain the preferential selectivity of SWNT onto Sephacryl, as opposed to other gels. Previously, amide groups have been shown to have an adsorption affinity for semiconducting SWNTs.[47] To further verify the specific functionality of Sephacryl allowing for SWNT separation, we added each of the two Sephacryl hydrogel precursor molecules, dextran and methyl bisacrylamide (MBA), to a 35 mM SDS suspension of (6,5) SWNT. We noted that for an addition of up to 100 mM dextran, there is no significant change in the absorption spectrum; however upon addition of 100 mM MBA, there was a $\sim$10 nm red-shift in the spectrum (Figure S2). This was true in both the presence (Figure S2,A and B) and absence (Figure S2,C and D) of the dextran, showing a direct interaction of the SWNT with the MBA and supporting our supposition that the amide functionality of Sephacryl is responsible for SWNT adsorption.

Finally, the hard-surface repulsion between a Sephacryl binding site and a semiconducting SWNT can be described by[48,49]

$$V_{\text{hard sphere}}(d) = \frac{A}{d^{12}} \tag{4}$$

where A is the hard-surface coefficient.

Given these contributions to eq 1, it is possible to consider the total system energy as a function of SWNT–Sephacryl separation distance d for a variety of relevant semiconducting SWNT chiralities. As, an example, the (6,5) chirality has a radius $r_{\text{SWNT}} = 0.379$ nm, using parameters $\sigma_{\text{SWNT}} = 1$ e$^-$/nm^2, $\sigma_{\text{SEPH}} = 0.1$ e$^-$/nm^2, $\varepsilon = 80$, $\kappa = 0.87$ nm (equivalent to 70 mM SDS), $l = 10$ nm (estimated SWNT length per Sephacryl binding site), $H_N = 481$ meV, $H_F = 538$ meV, $\beta = 0.15$, $r_0 = 0.4$ nm, and $A = 2.4 \times 10^{-13}$ meV nm^{12}, the contribution of $V_{\text{van der Waals}}$, $V_{\text{electrostatic}}$, and $V_{\text{hard sphere}}$ to the total $V(d)$ is depicted in Figure S8. A detailed discussion regarding the choice of specific parameters and the equations governing such are provided in the Supporting Information. This discussion includes sensitivity analyses for each unknown parameter, the data for which are included in Figures S3–S7.

As noted in Figure 1B, the total energy profiles are dominated by hard-surface repulsion at small distances ($d < 2$ Å), by van der Waals attraction at intermediate distances (2 Å $< d < 4$ Å), and by electrostatic repulsion at long distances (4 Å, $< d < 3$ nm); thermal energy dominates at distances greater than $\sim$3 nm. Note that hard-surface repulsion balances van der Waals attraction to produce a Lennard-Jones-like potential well, the bottom of which represents the surface–surface separation distance between a bound SWNT–Sephacryl pair, d_{bound}. Here, we do not account for an SDS layer between the nanotube and the Sephacryl in the bound state because the morphology

of SDS is known to be dynamic,[37] and a rigid-layer-like picture is likely inaccurate. We also note that the exact energy of the bound state predicted by eq 1 is an approximation, where a more complete picture of bound state energetics would necessarily include additional solvent effects such as water excluded by the bound SWNT, as well as the amide−SWNT interaction energy. However, there is no evidence for a semiconducting SWNT chiral dependence in these energies, and we find here that the electrostatic repulsion term is the most salient for determining chiral selectivity. Nevertheless, there is an opportunity to perform a more detailed *ab initio* calculation to fully understand this system, which is outside the scope of this work.

To model the rate at which semiconducting SWNTs bind to Sephacryl sites, we consider the total distance-dependent interaction profile for a given SWNT chirality (such as presented in Figure 1B) that governs the energetics of a binding event traversing from $d = \infty$, over the energetic barrier within the electrostatic repulsion-dominated region, and arriving at $d = d_{bound}$. Defining such a binding event as a collision, the rate constant associated with a particle traversing the energy profile $V(d)$ from $d = \infty$ to $d = d_{bound}$ developed by Fuchs[49,50] is given by

$$k_f = \frac{4\pi D}{\int_{d_{bound}}^{\infty} \frac{1}{d^2} e^{V(d)/k_B T} \, dd} \tag{5}$$

where k_B is the Boltzmann constant, T is absolute temperature, and D is the diffusion coefficient, determined using an adapted Einstein−Smoluchowski relation for a cylinder (SWNT)[51] in turbulent flow around a sphere (Sephacryl bead):[52]

$$D = k_B T \frac{\ln\left[\frac{L}{2 r_{SWNT}}\right] + 0.58}{3\pi\eta L}(2 + S_c^{2/5}\eta^{1/4}(0.4 Re^{1/2} + 0.06 Re^{2/3})) \tag{6}$$

Here, η is the dynamic viscosity of water, L is the length of the SWNT, and Sc and Re are the dimensionless Schmidt and Reynolds numbers, respectively.

Using the energy profile for the (6,5) chirality depicted in Figure 1B, eqs 5 and 6, and values of $L = 300$ nm, $T = 298$ K, $\eta = 1.0 \times 10^{-3}$ Pa·s, Sc = 1.1×10^{5}, and Re = 2.5×10^{5}, a reaction rate constant of 1.3×10^{-9} M^{-1} s^{-1} is calculated (see the Supporting Information for detailed calculation of Sc and Re). Interestingly, this binding rate constant is within an order of magnitude when compared with the $k_{6,5}$ published previously, obtained with an irreversible site-limited batch reactor model to describe Sephacryl-based separation of single-chirality (6,5) SWNT from a multichirality solution in 70 mM SDS.[27] To reconcile these two models, we consider the charge associated with the SWNT, σ_{SWNT}, which is a consequence of the incomplete association of Na$^+$ counterions with the SDS micelle surrounding the SWNT.[32] By altering the

associated charge from $\sigma_{SWNT} = 1$ e/nm^2 to $\sigma_{SWNT} = 0.94$ e/nm^2 and keeping all other parameters identical, one obtains an energy profile for the (6,5) SWNT associated with the experimentally determined second-order binding rate constant. This profile is integrated over distance using eq 6 to yield a reaction rate constant of $k_{(6,5)} = 6.4 \times 10^{-9}$ M^{-1} s^{-1}, a value that is nearly equivalent to that reported earlier for (6,5) SWNT binding to Sephacryl in 70 mM SDS.[27] Similarly, other chiralities' charge densities were adjusted to accurately fit the rate constants at 70 mM SDS adsorption, giving the energy profiles depicted in Figure 1B. It is important to note that throughout this work we assume an average SWNT length of $L = 300$ nm for all chiralities. Average length for the (6,5) chirality separated by this same methodology was determined experimentally using AFM,[5] the relatively short length of which is likely due to prolonged ultrasonication.[53] The sorting of SWNT by length remains an active and important area of research, and while the effects of SWNT length on surfactant-mediated gel separation are of potential importance to this methodology, such are beyond the scope of this work.

This study investigates the effects of SDS concentration on the process of SWNT adsorbing to Sephacryl binding sites. Specifically, the model developed here is used as a guide to understand the experimental observations presented in the following sections. While a complete understanding of the molecular dynamics governing these processes remains speculative, general agreement between our developed model and experimental results is demonstrated based on work by others regarding the morphology and charge state of SDS-wrapped SWNTs,[37−43] as well as previous zeta potential measurements of SDS-wrapped SWNTs.[43] We use the theory developed above to quantitatively predict the experimental adsorption kinetics of the separation process. Our findings both contribute to the basic understanding of the SDS-SWNT structure and inform ways to further improve and manipulate gel-based SWNT separation.

RESULTS AND DISCUSSION

The model formulated above provides a basis for the development of a molecular level mechanism describing gel-based SWNT separation, as guided by the experimental observations presented in the remainder of this work. Specifically, we quantitatively outline the effects of perturbing SWNT solution starting material (by varying the duration of both ultrasonication and ultracentrifugation) and SDS surfactant concentration on the resulting single-chirality semiconducting SWNT separation. Empirical results of each perturbation are compared with model predictions, providing mechanistic insights into the separation process.

Effect of Surfactant Concentration on SWNT Adsorption to Sephacryl. The effect of SDS concentration on surfactant morphology around SWNTs has been the subject of
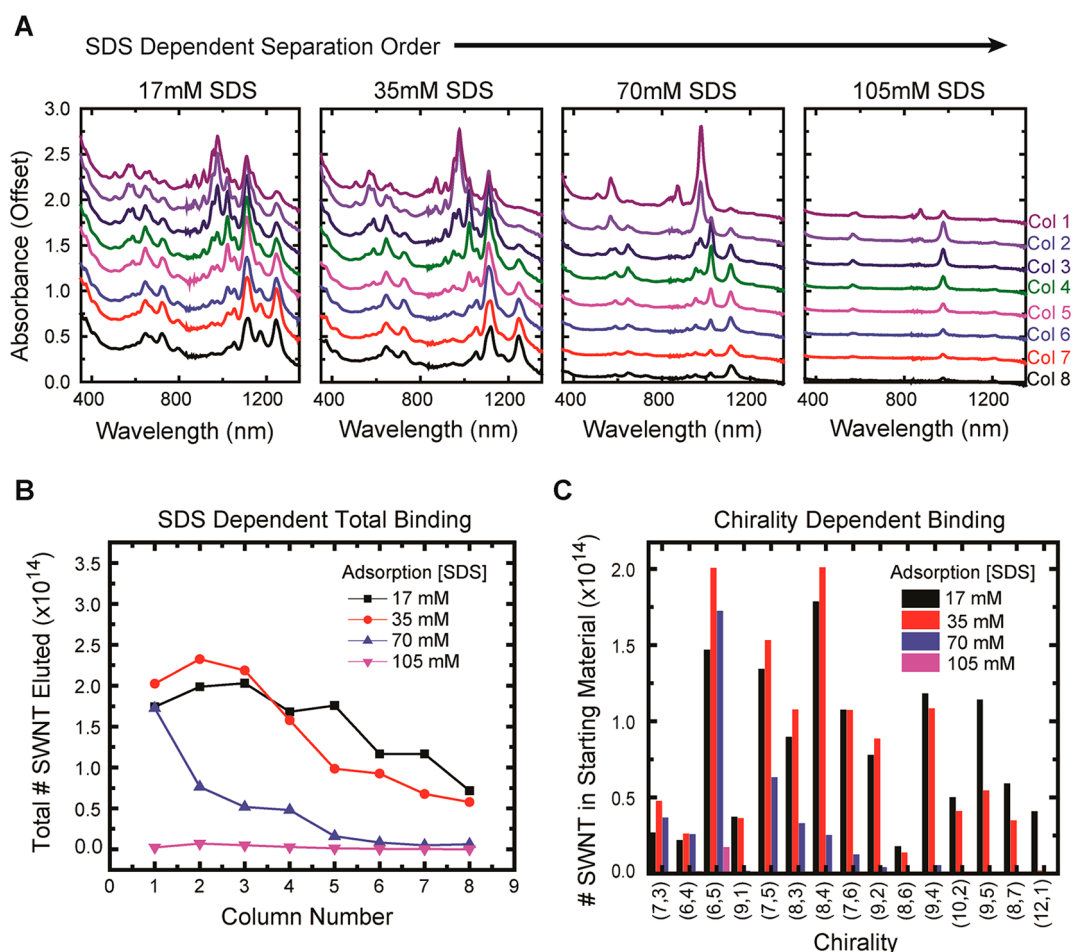
Figure 2. (A) Offset absorbance spectra of the eluted SWNT from various starting SDS concentrations, showing that as the SDS concentration is increased the distribution and number of SWNTs that bind are reduced. (B) Total SWNT per column for each SDS concentration showing generally that at lower SDS concentrations there is a lower SWNT adsorption. (C) Bar graph showing the total number of separated SWNTs per chirality for each SDS concentration. Note that the number of SWNTs separated is highly dependent on SDS concentration, as predicted.

various studies. For example, the morphology of the SDS layer on a semiconducting SWNT is known to be affected strongly by both SDS concentration and solution ionic strength.[37,39] Further, it has been shown that the morphology of SDS on metallic SWNT is relatively static *versus* SDS concentration and is expected to have a saturated (maximum limit of SDS associated with the SWNT surface) structure, even at low concentrations.[37] Even more significant is the prediction that different semiconducting SWNT chiralities have different concentrations at which the surfactant structure saturates.[37] Further, the SDS concentration dependent surfactant morphology, which is unique for semiconducting *versus* metallic SWNTs and for different chiralities within the semiconducting SWNT family, is believed to be the underlying phenomenon responsible for SWNT separation using density gradient ultracentrifugation, where the buoyant density of SWNT is highly dependent on surfactant packing.[16,39,54]

Similarly, we find here that the surfactant concentrations, and presumably the surfactant structure, play a central role in the selectivity of a gel to bind various

chiralities of SWNTs. To demonstrate this effect, we prepared SWNT suspensions in the presence of 17, 35, 70, and 105 mM SDS, each of which was ultrasonicated for 20 h at 20 W and ultracentrifuged at 187000*g* for 4 h. Each sample was then used as the starting material for an eight-column gel-based separation. In each case, the Sephacryl gel and subsequent rinse steps were equilibrated to the same SDS concentration as the SWNT solution. For each column of each SDS concentration, 175 mM SDS was used to elute the bound SWNT from the gel. The absorbance spectra of eluted samples from this process are shown in Figure 2A, while quantitative analyses of these spectra presented using background-subtracted Lorentzian line shape fitting are shown in Figure 2B and C.

In this analysis, we note that when separated from solutions of lower SDS concentration, the number of SWNTs (Figure 2B), distribution of chiralities that are adsorbed within each column, and the total number of separable chiralities all increase (Figure 2C). For example, in the 17 and 35 mM SDS separations, we observe the additional presence of larger diameter SWNTs,

TABLE 1. List of All Binding Rate Constants, $k_{n,m}$, Determined Here Using the Model Outlined in Ref 27 along with per Unit-Length Charge ξ (e^-/nm) Associated with All SWNT Chiralities Identified Here, Using the Model Outlined in the Model Section above and eq 7, under Four Different SDS Surfactant Concentrations[a]

(n,m)	18 mM SDS		35 mM SDS		70 mM SDS		105 mM SDS	
	$k_{n,m}$ (M_θ^{-1} s^{-1})	ξ (e^-/nm)	$k_{n,m}$ (M_θ^{-1} s^{-1})	ξ (e^-/nm)	$k_{n,m}$ (M_θ^{-1} s^{-1})	ξ (e^-/nm)	$k_{n,m}$ (M_θ^{-1} s^{-1})	ξ (e^-/nm)
(7,3)	2.8×10^{-6}	0.41	1.8×10^{-6}	0.86	1.7×10^{-6}	1.47		
(6,4)	2.7×10^{-6}	0.41	2.7×10^{-6}	0.79	2.9×10^{-7}	1.74	1.6×10^{-9}	2.85
(6,5)	1.1×10^{-6}	0.51	6.7×10^{-7}	1.00	6.4×10^{-9}	2.23	2.4×10^{-11}	3.32
(9,1)	1.4×10^{-6}	0.48	1.8×10^{-7}	1.16				
(7,5)	4.5×10^{-7}	0.60	1.5×10^{-7}	1.19	1.5×10^{-11}	2.82		
(8,3)	1.1×10^{-6}	0.51	3.3×10^{-7}	1.09	2.2×10^{-9}	2.35		
(8,4)	3.8×10^{-7}	0.62	1.7×10^{-7}	1.18	1.6×10^{-11}	2.83		
(7,6)	1.9×10^{-7}	0.68	1.2×10^{-7}	1.23	6.6×10^{-12}	2.95		
(9,2)	3.7×10^{-7}	0.62	1.2×10^{-7}	1.22				
(8,6)	1.1×10^{-7}	0.73	1.0×10^{-7}	1.27				
(9,4)	2.7×10^{-7}	0.65	1.2×10^{-7}	1.24				
(10,2)	1.2×10^{-7}	0.73	9.5×10^{-8}	1.26				
(9,5)	1.7×10^{-7}	0.69	9.8×10^{-8}	1.27				
(8,7)	1.8×10^{-7}	0.69	9.6×10^{-8}	1.29				
(12,1)	4.9×10^{-8}	0.81	3.2×10^{-9}	1.63				

[a] Note that values for $k_{n,m}$ and ξ (e^-/nm) not listed here at 70 and 105 mM are absent because corresponding SWNT chiralities were not separated at the time scale under investigation here.

such as the (8,7) and (12,1) chiralities. However, these species are not separated from solutions of higher SDS concentration: at 105 mM SDS only the (6,4) and (6,5) chiralities are separated. Hence, there is a large discrepancy in which SWNT chiralities are separable based on the SDS concentration of the SWNT suspension. This finding implies the presence of a chirality-dependent strength of SWNT−Sephacryl affinity, to the extent that there exists a maximum SDS concentration for the separability of each SWNT chirality on the time scale of this experiment.

In order to analyze the differences in adsorption at different SDS concentrations, we use the theory developed in this work to propose a molecular level picture of the system in each case. As described above, this analysis begins by fitting the absorption spectra of a multicolumn separation to quantify the presence of each chirality within each column of separation, as described previously[27] and shown for this work in Figure S9. Such quantities are then subject to a second-order forward reaction binding model[27] to yield binding rate constants, $k_{n,m}$(SDS), between a Sephacryl gel binding site and each experimentally extracted chirality, which we explicitly write here as being SDS concentration dependent. The chirality and SDS concentration dependent binding rate constants for the four SDS concentrations under investigation are listed in Table 1, where we note that rate constants calculated at 70 mM SDS are nearly identical to our previous study conducted under these conditions, where surfactant concentration was not explored.[27]

As an example, we show the best fits of this analysis (lines) in direct comparison with experimental elution quantities (solid squares) for the separation performed in 17 mM SDS, Figure 3A; those for the other three surfactant concentrations are shown in Figure S9. From the calculated chirality and SDS concentration dependent adsorption rate constants, we apply the model developed earlier in this work, whereby the SWNT surface charge density is the primary variable governing the height of the barrier that the system must cross to undergo a binding event. The energy barrier dictates the rate at which each SWNT chirality adsorbs to the gel and, therefore, the chirality composition of each column. Because this barrier height is physically correlated with the electrostatic repulsion between the like-charged amide binding site and surfactant-surrounded SWNT, a relatively larger SWNT charge density corresponds to a relatively higher activation barrier for the binding event.

In order to relate experimentally derived binding rate constants with molecular-scale dynamics, we matched the modeled binding rate constant (from eq 5) with that predicted by our second-order selective binding analysis using a best-fit analysis, assigning SWNT surface charge density as the only free parameter. To relate the fitted SWNT surface charge density, σ_{SWNT} (e^-/nm^2), to a more geometrically clear chirality-independent parameter, we define here SWNT effective linear charge density, $\xi_{n,m}$ (e^-/nm), outlined by the following relationship:

$$\xi_{n,m} = 2\pi r_{SWNT}\sigma_{SWNT} \qquad (7)$$

This analysis demonstrates that by assuming a chirality and SDS concentration dependent charge on each semiconducting SWNT, which are in turn derived from
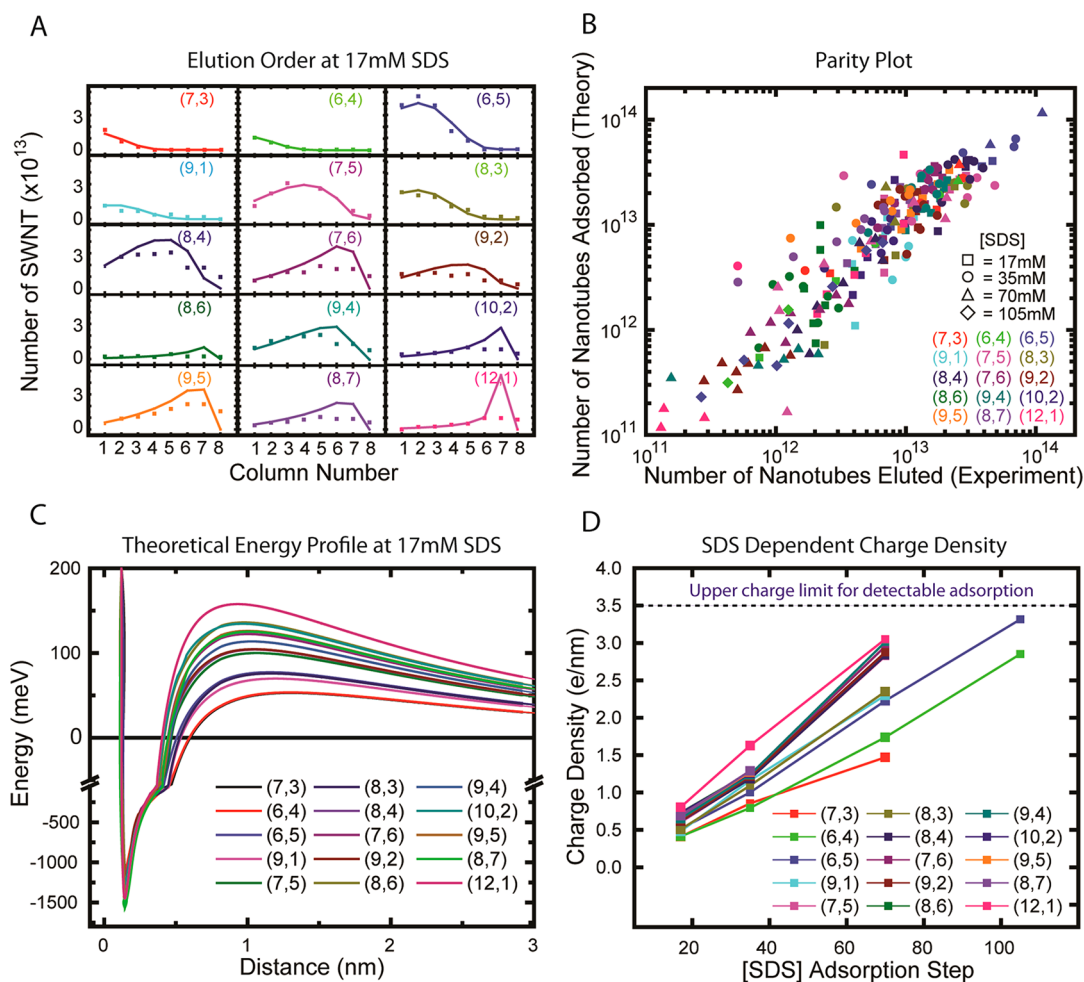
Figure 3. (A) Panels showcasing the fit of a kinetic model to the elution of each chirality for the 17 mM SDS solution elution profile. Solid squares are experimental data, and lines are theoretical fits. (B) Parity plot comparing the number of tubes adsorbed based on our theory *vs* the measured eluted SWNT. (C) Energy profiles of each chirality of SWNT for the 17 mM adsorption as modeled to fit the elution data. (D) Charge density for each SWNT as a function of the SDS concentration in which it is equilibrated.

the incomplete cationic association of Na^+ with the SWNT-associated SDS anion, it is possible to describe the single-chirality gel-based SWNT separation in terms of molecular-scale interactions. A summary parity plot comparing the number of tubes adsorbed based on our theory *versus* the measured eluted SWNT shows excellent agreement (Figure 3B). The chirality-dependent system energy as a function of SWNT–Sephacryl separation distance for all 15 chiralities separated from a SWNT solution in 17 mM SDS is shown in Figure 3C, while the chirality and SDS concentration dependent SWNT charge density for all four SDS concentrations investigated is shown graphically in Figure 3D and listed numerically in Table 1.

In order to compare the results listed in Table 1 with previous experimental findings, we translated the charge densities listed here at 35 mM SDS to equivalent zeta potentials, using Debye–Huckel theory for a cylinder[55] and assuming that the zeta potential is equivalent to the surface potential. Using this method, zeta potentials of between 30 and 60 mV are predicted

from our SWNT surface charges, which range from 0.86 to 1.63 e^-/nm in 35 mM SDS. These potentials fall within the range of previously published experimental zeta potential measurements by others of 35 mM SDS wrapped SWNTs (mean of 80 mV),[43] where chiral inhomogeneity could be responsible for the breadth of the zeta potential measurement ($\pm$20 mV). The excellent agreement between our calculated charge density value and experimentally validated values provides further evidence for the validity of charge densities calculated using this theory and the assignment of such charges as the underlying factor affording single-chirality SWNT separation.

As can be seen in Figure 3D, the surface charge density of each SWNT chirality is predicted to increase in a chirality-dependent manner with increasing SDS surfactant concentration. Also, we note the presence of a chirality-dependent charge density at which the energy barrier height associated with a binding event becomes sufficiently large as to prevent the binding of that species on the time scale utilized here. This charge

density, which we define as resulting in an effective binding rate constant of $10^{-13}\,M^{-1}\,s^{-1}$ or lower, occurs at approximately 3.5 e⁻/nm or greater and varies slightly depending on chirality. We postulate that at surfactant concentrations above this point SDS undergoes a morphological transition and the surfactant wrapping around a given SWNT becomes effectively saturated, preventing the SWNT surface from interacting with the Sephacryl binding site on the time scale of this experiment and therefore limiting the number of separable chiralities (particularly those of large diameter) at SDS concentrations of ≥70 mM.

We use the above analysis to understand the influence of the change in SWNT charge state in the context of gel-based single-chirality semiconducting SWNT separation. We hypothesize that at low SDS concentrations, where a large quantity and distribution of SWNTs adsorb to the Sephacryl gel, there exist only minor differences in the SDS morphology around those SWNT species, leading to similar chirality-dependent surface charge densities, similar binding affinities, and low per-column selectivity. Specifically, at relatively low SDS concentration we expect that the SDS is less densely packed around the nanotube, which spatially allows the system to accommodate more Na⁺ counterions. The increased cation concentration effectively negates the charge imbalance associated with the SWNT−surfactant complex and reduces the relative difference in electrostatic repulsive forces between different SWNT chiralities. The resultant low chiral selectivity can be seen in Figure 2A, 17 mM SDS.

As the SDS concentration is increased from 17 mM to 105 mM, we expect that the chirality dependency in counterion association becomes more pronounced. There are two important aspects to this predicted change: (1) that the charge increases for all semiconducting SWNT chiralities and (2) that this increase is chirality dependent. We hypothesize that each SWNT chirality displays different SDS packing morphologies dependent on surrounding SDS concentration and predict that chiralities not separated at larger SDS concentration are limited by SDS morphology saturation at that concentration. The resultant separation is highly chirally selective, but unable to separate large-diameter SWNTs (Figure 2A, 105 mM).

To further understand the mechanism of the change in SDS morphology *via* concentration, we increased the counterion concentration by performing two simultaneous separations, one in which the SWNTs were eluted with 105 mM SDS and the other with 105 mM NaCl. In this experiment, all other conditions were held constant as described in the Methods section. The elution profiles of these were very similar (Figure S10), showing that the ionic strength of the solution has a direct effect on the morphology of the SDS, independent of SDS concentration. It is important to note that prior to elution the system still has SDS present in the gel, which is what allows the morphology change despite not adding the higher concentration SDS. To ensure that this is the case, we further controlled the experiment by running a simultaneous experiment where we first attempted to elute with water, clearing the gel of all SDS. We then attempted to elute with just 105 mM NaCl and finally after that with 5% SDS. In neither the water nor NaCl elutions did we observe any SWNT elute, and upon addition of SDS, some SWNT do elute, though not as much likely due to the increased binding between the SWNT and Sephacryl upon removal of the SDS completely (Figure S10). This observation provides further evidence for the molecular picture of a morphology-induced electrostatic change leading to the chiral separation. The influence of NaCl on SDS-wrapped nanotubes has been observed optically in previous studies, where SDS morphology was assumed to be the driver of the observed change.[37] Recent work by Hennrich and co-workers also shows that the charge of the system around the SWNT greatly affects the SDS morphology, such that the introduction of just 5 µM 1-dodecanol to the SWNT prevents it from binding to the Sephacryl gel completely.[30] The experiment presented in this work supports work by others demonstrating the dynamic nature of SDS morphology on SWNTs, which is significant to our understanding of the Sephacryl gel-based separation.

This mechanism can also be used to explain why metallic SWNTs do not adsorb to the gel, an observation made in the foundational studies using gels to separate SWNTs.[26] Because the SDS morphology saturation has been shown to occur in metallic SWNTs at even lower surfactant concentrations,[37] the activation barrier for metallic SWNT binding with Sephacryl gel is too high for the SWNTs to have an affinity for the gel. Further investigations, likely using chirality-dependent SWNT simulations at the molecular scale, are necessary to verify our postulation of chirality- and concentration-dependent morphology of the SWNT−surfactant complex. The prediction of such a phenomenon using *ab initio* calculations would allow for more precise modeling of SWNT separation and inform the mechanism behind both gel-based and density gradient nanotube separation techniques.

Varying Ultrasonication Duration. As specified in the Methods section, the bulk SWNT solution from which single-chirality material is separated is prepared by weighing out (100 mg) solid SWNT starting material and suspending it in an aqueous SDS surfactant solution *via* 1/2 in. tip ultrasonication at 20 W. While the standard procedure for this preparation calls for 20 h of ultrasonication, important insight into the separation mechanism is gained through systematically varying ultrasonication duration and keeping all other separation conditions constant (2 h ultracentrifugation at 187000g, 70 mM SDS). The absorbance profiles of ultracentrifuged samples sonicated for 1−18 h are
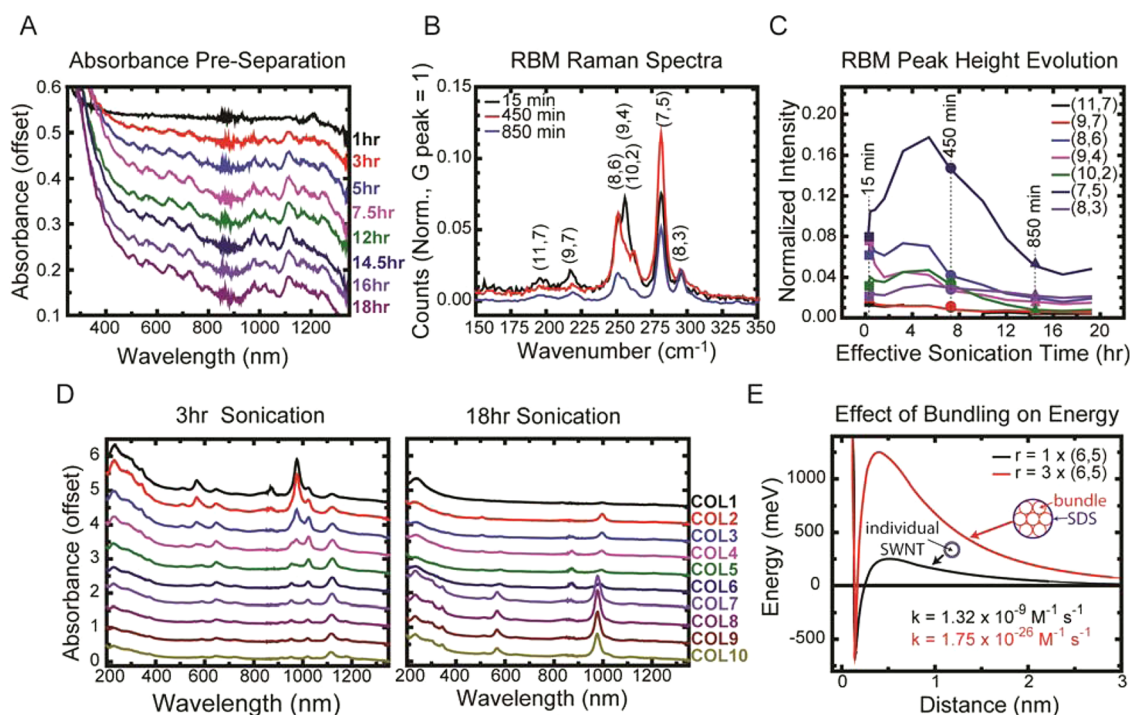
Figure 4. (A) Offset absorbance spectra of the SWNTs immediately before separation for various sonication times. (B) Radial breathing mode (RBM) section of the Raman spectra for three specific effective sonication times here shown as 15, 450, and 850 min. (C) Peak heights of the RBM peaks of various SWNT chiralities, normalized to the G-peak height, as a function of sonication time, showing a clear evolution of relative heights with time. (D) Offset absorbance spectra of the separations carried out on SWNT that were sonicated for 3 and 18 h, showing differences in separation based on sonication time. (F) Energy profiles for a bundle of (6,5) SWNT compared to that of an individual (6,5) SWNT.

shown in Figure 4A. With increasing sonication time, the E_{11} peaks in the nIR region of the spectrum become more distinct, while the background absorbance decreases, indicating that the ratio of individually dispersed SWNTs to other carbon materials (including SWNT bundles) increases with prolonged ultrasonication.[56]

In addition, we use Raman spectroscopy to track the evolution of peaks located in the radial breathing mode (RBM) region (150–350 cm^{-1}) with increasing sonication time; each spectrum is normalized to the height of the G peak (~1590 cm^{-1}), Figure 4B. The noted Raman RBM peaks, each of which corresponds to a unique SWNT chirality, change in height over the course of the 18 h sonication procedure and can be used to track and assess the relative sonication state of a colloidal SWNT suspension, Figure 4C. The origin for the evolution of the SWNT RBM spectrum during ultrasonication is assigned to SWNT debundling, or an overall increase in the number of individual SWNT in the dispersion, as demonstrated previously by Heller *et al.* when using SWNT under varying bundling conditions.[56] Continued evolution of relative RBM peak heights over the course of an 18 h sonication further exemplifies the necessity of relatively long sonication periods to more completely debundle SWNTs.

Following ultrasonication (1–18 h) and subsequent ultracentrifugation, each SWNT starting material was subject to the aforementioned separation procedure.

The per-column elutions of the two extreme cases, 3 and 18 h, are shown in Figure 4D, while intermediate times are presented in Figure S11. As the sonication time is increased, the separation changes from several chiralities in each column with fewer numbers of a given chirality to highly pure single chiralities with each chirality's total number increasing.

This observation is consistent with the assumption that increasing duration of the ultrasonication step prior to SWNT separation results in the individualization of more SWNT from their as-received bundled state. At short sonication time (Figure 4D, 3 h sonication) only a small fraction of each chirality has been debundled, and relatively less amorphous carbon fragments have been generated,[27] which translates to a separation whereby an overabundance of binding sites in the first several columns are occupied by nonspecific-chirality SWNT, and little SWNT content is separated from later columns. In contrast, at long sonication time (Figure 4D, 18 h sonication) a larger fraction of each chirality has been debundled, and significantly more amorphous carbon fragments have been generated, resulting in domination of the first several columns by amorphous carbon fragments (which have been shown to have binding constants to Sephacryl gel much greater than semiconducting SWNTs[27] which do not show spectroscopic signatures) and highly pure semiconducting SWNT content in later columns.
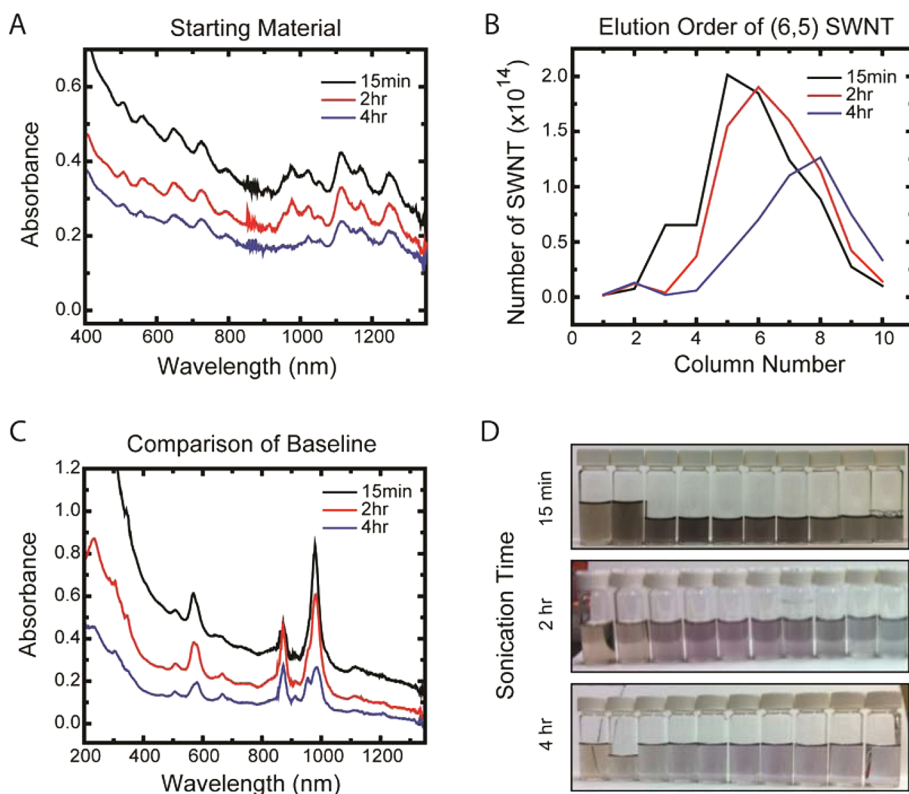
Figure 5. (A) Absorbance spectra of the SWNT immediately before separation for various sonication times. (B) The peak height per column of the (6,5) SWNT for the different centrifugation times, showing very small differences in quantity and almost no difference in separation trend. (C) Absorbance spectra of column 3 for the three different centrifugation times, showing large baseline differences. (D) Photographs of the elutions from the three different centrifugation times, showing that a lower baseline leads to color differentiation as chirality distribution changes.

This description of bundle-driven selective separation presumes that only single-chirality SWNTs bind to Sephacryl gel, an assertion suggested by others[26,27] without offering a mechanistic picture. To understand the origins of this phenomenon quantitatively, we apply the theory developed in this work to calculate the system energy as a function of SWNT−Sephacryl separation distance for a SWNT bundle of seven like-chirality SWNTs, Figure 4E. Assuming that a bundle of seven SWNTs can be effectively modeled as a single SWNT with three times the diameter and identical surface charge density, SWNT bundling results in a predicted interaction potential with a significantly larger barrier height, which effectively prevents the binding of a relatively small seven-SWNT bundle to a Sephacryl gel binding site. This explains and demonstrates the importance of the ultrasonication step, where atypically long sonication times (∼20 h) are necessary to improve the selectivity and yield of the separation process.

It is important to note that along with bundle dynamics prolonged sonication is also known to result in nanotube cutting,[53] which has been shown to both reduce and narrow the length distribution of solution-phase SWNTs.[57] Experimentally, it remains unclear how to deconvolute SWNT cutting from SWNT bundle reduction in terms of solution-phase Sephacryl gel interactions, as the generation of solution-phase SWNTs requires ultrasonication, which necessarily both cuts and debundles SWNTs. While all observations and analysis here are consistent with a change in bundling state, and not a change in length distribution, as the predominant mechanism for ultrasonication effect on semiconducting SWNT separation, methodological progress in SWNT length sorting is necessary to more fully understand its effect on this process and could serve as a valuable extension to the model and work presented here.

Varying Ultracentrifugation Duration. Following ultrasonication, SWNT suspensions are typically subjected to ultracentrifugation and retention of only the top fraction, with the ultimate intent of increasing the ratio of individually suspended SWNTs in the solution. To investigate the effects of this practice on the outcome of a single-chirality SWNT separation, we sonicated three SWNT solutions for 20 h each at 20 W and ultracentrifuged the samples at 187000*g* for 15 min, 2 h, and 4 h, respectively. The absorbance spectra of these samples show a reducing baseline with increasing centrifugation time, Figure 5A, as is consistent with the expectation that ultracentrifugation can effectively separate individually dispersed SWNTs from the rest of the carbonaceous materials, which are known to have a relatively featureless, sloping baseline.[58] It is

important to note that, in addition to removing SWNT bundles and carbonaceous impurities from the solution, prolonged ultracentrifugation also effectively reduces the total SWNT content—or overall SWNT concentration—of the solution that is used to perform the gel separaiton. Although previous findings suggest that separation dynamics should be affected primarily by the concentration of individualized SWNTs, and not by total SWNT concentration, we explored this variation through a control experiment whereby 10 columns of separation were performed. SWNT concentration alone was varied, and all other parameters such as SDS concentration, total SWNT content, and total per-column SWNT/Sephacryl interaction time were held constant. This control demonstrated that at initial SWNT concentrations of 0.25, 0.50, and 1.00 mg/mL the resultant separated SWNTs did not vary significantly over 10 columns, as shown in Figure S12.

Using these three suspensions shown in Figure 5A as starting materials, we performed a standard separation of 10 columns for each sample. Remarkably, there is not significant variation in either the per-column chirality distribution or total SWNT amount, Figure 5B. However, we note that increased centrifugation (lower initial baseline absorbance) yields eluted suspensions that also show an overall lower baseline in the absorbance spectrum; that is, there is less carbon impurity as centrifugation time is increased. This is evident both in the absorbance spectra of a selected common column (column 5 is shown in Figure 5C) and through visual inspection of the 10 column elutions, with sample color becoming more distinct as the carbon impurity content decreases, Figure 5D. Although increased carbonaceous material does not appear to significantly affect the resultant SWNT separation, its effect on performance of devices constructed from purified SWNTs remains unclear and is the subject of an ongoing investigation.

CONCLUSION

We have demonstrated the use of a quantitative theory for the prediction of single-chirality SWNT gel based separation. This description ultimately relates experimentally observed binding rate constants with a chirality and SDS concentration-dependent surface charge density associated with semiconducting SWNTs. Building a molecular-scale mechanistic model for the gel-based SWNT separation process affords a more complete understanding of the various factors that influence this process and provides insight into the dynamic and important role that surfactant morphology plays. This work develops foundational theoretical principles toward the eventual realization of industrial-scale, high-yield, high-purity, single-chirality semiconducting SWNT separation.

METHODS

Preparation of Aqueous SWNT Suspension. In order to prepare the SWNT solutions used in this work, we follow the gel-based separation procedure previously described,[27] modified from the method published by Kataura and co-workers.[26] Raw HiPco SWNT (Unidym, lot: R1831) was first processed using the organic—aqueous phase separation suggested by the manufacturer for the creation of solid SWNT material, which we homogenize and grind with a mortar-and-pestle to create the fine powder used as our starting SWNT material. The SWNT powder is weighed (100 mg) and dispersed in 100 mL of aqueous sodium dodecyl sulfate (Sigma 98%) solution at the SDS concentration of interest (17—105 mM). This solution is homogenized via bath sonication (Branson 2510) for 5 min and placed into a temperature-controlled bath held at 5 °C and sonicated using a Branson 1/2 in. tip sonicator (Branson Digital Sonifier 250, Cole Parmer 04710-40 1/2 in. tip placed ~10 mm from bottom of beaker and total per-tip use regulated to <100 h) at 20 W for a duration ranging from 2 to 20 h, as specified.

Following ultrasonication, the sample contains individually suspended SWNT, SWNT bundles, and other amorphous carbon material.[27,58] The presence of bundles is minimized via ultracentrifugation at 187000g (32 000 rpm, Beckman Coulter Optima L100 XP, SW 32 Ti rotor, Beckman 344058 40 mL tubes) for 15 min to 4 h, as specified. The top 90% of the supernatant is used immediately as the initial sample for the primary pass single-chirality semiconducting SWNT separation procedure described below.

Primary Pass Single-Chirality Semiconducting SWNT Separation. The procedure used to perform the separation of SWNTs very closely follows the separation developed in our previous work.[27] However, in this study we vary one of the following aspects of the initial SWNT solution: sonication time, centrifugation time, or SDS concentration. In each case 10 mL of the solution is passed through 1.4 mL of Sephacryl S200 gel (equilibrated to the same SDS concentration as the SWNT solution) at a rate of 1 mL/min, regulated by syringe-pump-controlled overpressure. Unabsorbed solution is collected as the "flow through", which is used as the starting solution for the following iterative column. After washing the Sephacryl with 4 mL of SDS solution equivalent in concentration to the initial SWNT solution, adsorbed nanotubes are eluted and collected by passing 175 mM SDS through the gel. Fresh Sephacryl is loaded into a new column, and this process is iterated to yield the specified number of "separation columns" referred to here.[27]

Absorbance Spectroscopy and SWNT Distribution Analysis. Absorbance spectroscopy (Shimadzu UV-3101PC) is used to analyze the chirality distribution of the separated SWNT samples produced by the gel separation method. The lowest-energy E_{11} absorbance peaks are fit using Lorentzian line shapes after performing a manual background subtraction to minimize any broad absorbance features that do not correlate with SWNT absorption, Figure S1. The fitted peak heights are used to determine the quantity of each SWNT chirality in the sample using the per-carbon-atom absorbance cross section of the (6,5) chirality,[59] as absorbance cross section values for other SWNTs have not been determined experimentally to date.

Binding Rate Constant Determination. The separation and quantification procedures described above are iterated to yield various chirality distributions for each iterative column under specified separation conditions. We have previously shown that this separation procedure behaves as a well-mixed batch reactor, which can be described using second-order forward adsorption kinetics.[27] Specifically, a fixed number of Sephacryl binding sites are assigned to each separation column, which interacts with the separable semiconducting SWNT present in the starting solution in a manner dictated by second-order kinetics. A unique binding rate constant $k_{n,m}$ is determined for each SWNT chirality, which is responsible for the overall separation order and relative yield of semiconducting SWNTs per gel column.[27,47] Here, this model is used to determine the binding

rate constant for each separable chirality under specified run conditions in an identical manner to what was done previously for standard separation conditions.[27]

REFERENCES AND NOTES

1. Liu, Z.; Tabakman, S.; Welsher, K.; Dai, H. Carbon Nanotubes in Biology and Medicine: *In Vitro* and *in Vivo* Detection, Imaging and Drug Delivery. *Nano Res.* **2009**, *2*, 85–120.
2. Boghossian, A. A.; Zhang, J.; Barone, P. W.; Reuel, N. F.; Kim, J.-H.; Heller, D. A.; Ahn, J.-H.; Hilmer, A. J.; Rwei, A.; Arkalgud, J. R.; *et al.* Near-Infrared Fluorescent Sensors Based on Single-Walled Carbon Nanotubes for Life Sciences Applications. *ChemSusChem* **2011**, *4*, 848–863.
3. Avouris, P.; Freitag, M.; Perebeinos, V. Carbon-Nanotube Photonics and Optoelectronics. *Nat. Photonics* **2008**, *2*, 341–350.
4. Opatkiewicz, J.; LeMieux, M. C.; Bao, Z. N. Nanotubes on Display: How Carbon Nanotubes Can Be Integrated into Electronic Displays. *ACS Nano* **2010**, *4*, 2975–2978.
5. Jain, R. M.; Howden, R.; Tvrdy, K.; Shimizu, S.; Hilmer, A. J.; McNicholas, T. P.; Gleason, K. K.; Strano, M. S. Polymer-Free Near-Infrared Photovoltaics with Single Chirality (6,5) Semiconducting Carbon Nanotube Active Layers. *Adv. Mater.* **2012**, *24*, 4436–4439.
6. Bindl, D. J.; Wu, M. Y.; Prehn, F. C.; Arnold, M. S. Efficiently Harvesting Excitons from Electronic Type-Controlled Semiconducting Carbon Nanotube Films. *Nano Lett.* **2011**, *11*, 455–460.
7. Avouris, P.; Chen, J.; Freitag, M.; Perebeinos, V.; Tsang, J. C. Carbon Nanotube Optoelectronics. *Phys. Status Solidi B* **2006**, *243*, 3197–3203.
8. Bindl, D. J.; Arnold, M. S. Efficient Exciton Relaxation and Charge Generation in Nearly Monochiral (7,5) Carbon Nanotube/C60 Thin-Film Photovoltaics. *J. Phys. Chem. C* **2013**, *117*, 2390–2395.
9. Bindl, D. J.; Brewer, A. S.; Arnold, M. S. Semiconducting Carbon Nanotube/Fullerene Blended Heterojunctions for Photovoltaic Near-Infrared Photon Harvesting. *Nano Res.* **2011**, *4*, 1174–1179.
10. Bindl, D. J.; Safron, N. S.; Arnold, M. S. Dissociating Excitons Photogenerated in Semiconducting Carbon Nanotubes at Polymeric Photovoltaic Heterojunction Interfaces. *ACS Nano* **2010**, *4*, 5657–5664.
11. Behabtu, N.; Green, M. J.; Pasquali, M. Carbon Nanotube-Based Neat Fibers. *Nano Today* **2008**, *3*, 24–34.
12. Behabtu, N.; Young, C. C.; Tsentalovich, D. E.; Kleinerman, O.; Wang, X.; Ma, A. W. K.; Bengio, E. A.; ter Waarbeek, R. F.; de Jong, J. J.; Hoogerwerf, R. E.; *et al.* Strong, Light, Multifunctional Fibers of Carbon Nanotubes with Ultrahigh Conductivity. *Science* **2013**, *339*, 182–186.
13. Lee, A. J.; Wang, X.; Carlson, L. J.; Smyder, J. A.; Loesch, B.; Tu, X.; Zheng, M.; Krauss, T. D. Bright Fluorescence from Individual Single-Walled Carbon Nanotubes. *Nano Lett.* **2011**, *11*, 1636–1640.
14. Nish, A.; Hwang, J.-Y.; Doig, J.; Nicholas, R. J. Highly Selective Dispersion of Single-Walled Carbon Nanotubes Using Aromatic Polymers. *Nat. Nanotechnol.* **2007**, *2*, 640–646.
15. Ghosh, S.; Bachilo, S. M.; Weisman, R. B. Advanced Sorting of Single-Walled Carbon Nanotubes by Nonlinear Density-Gradient Ultracentrifugation. *Nat. Nanotechnol.* **2010**, *5*, 443–450.
16. Arnold, M. S.; Green, A. A.; Hulvat, J. F.; Stupp, S. I.; Hersam, M. C. Sorting Carbon Nanotubes by Electronic Structure Using Density Differentiation. *Nat. Nanotechnol.* **2006**, *1*, 60–65.
17. Green, A. A.; Duch, M. C.; Hersam, M. C. Isolation of Single-Walled Carbon Nanotube Enantiomers by Density Differentiation. *Nano Res.* **2009**, *2*, 69–77.
18. Green, A. A.; Hersam, M. C. Nearly Single-Chirality Single-Walled Carbon Nanotubes Produced *via* Orthogonal Iterative Density Gradient Ultracentrifugation. *Adv. Mater.* **2011**, *23*, 2185–2190.
19. Tu, X. M.; Manohar, S.; Jagota, A.; Zheng, M. DNA Sequence Motifs for Structure-Specific Recognition and Separation of Carbon Nanotubes. *Nature* **2009**, *460*, 250–253.
20. Zheng, M.; Jagota, A.; Strano, M. S.; Santos, A. P.; Barone, P.; Chou, S. G.; Diner, B. A.; Dresselhaus, M. S.; McLean, R. S.; Onoa, G. B.; *et al.* Structure-Based Carbon Nanotube Sorting by Sequence-Dependent DNA Assembly. *Science* **2003**, *302*, 1545–1548.
21. Tanaka, T.; Liu, H.; Fujii, S.; Kataura, H. From Metal/Semiconductor Separation to Single-Chirality Separation of Single-Wall Carbon Nanotubes Using Gel. *Phys. Status Solidi RRL* **2011**, *5*, 301–306.
22. Moshammer, K.; Hennrich, F.; Kappes, M. M. Selective Suspension in Aqueous Sodium Dodecyl Sulfate According to Electronic Structure Type Allows Simple Separation of Metallic from Semiconducting Single-Walled Carbon Nanotubes. *Nano Res.* **2009**, *2*, 599–606.
23. Reich, S.; Thomsen, C.; Maultzsch, J. *Carbon Nanotubes - Basic Concepts and Physical Properties*, 1st ed.; Wiley-VCH: Weinheim, 2004.
24. Arnold, M. S.; Zimmerman, J. D.; Renshaw, C. K.; Xu, X.; Lunt, R. R.; Austin, C. M.; Forrest, S. R. Broad Spectral Response Using Carbon Nanotube/Organic Semiconductor/C60 Photodetectors. *Nano Lett.* **2009**, *9*, 3354–3358.
25. Diao, S.; Hong, G.; Robinson, J. T.; Jiao, L.; Antaris, A. L.; Wu, J. Z.; Choi, C. L.; Dai, H. Chirality Enriched (12,1) and (11,3) Single-Walled Carbon Nanotubes for Biological Imaging. *J. Am. Chem. Soc.* **2012**, *134*, 16971–16974.
26. Liu, H. P.; Nishide, D.; Tanaka, T.; Kataura, H. Large-Scale Single-Chirality Separation of Single-Wall Carbon Nanotubes by Simple Gel Chromatography. *Nat. Commun.* **2011**, *2*.
27. Tvrdy, K.; Jain, R. M.; Han, R.; Hilmer, A. J.; McNicholas, T. P.; Strano, M. S. A Kinetic Model for the Deterministic Prediction of Gel-Based Single-Chirality Single-Walled Carbon Nanotube Separation. *ACS Nano* **2013**, *7*, 1779−1789.
28. Liu, H.; Tanaka, T.; Urabe, Y.; Kataura, H. High-Efficiency Single-Chirality Separation of Carbon Nanotubes Using Temperature-Controlled Gel Chromatography. *Nano Lett.* **2013**, *13*, 1996–2003.
29. Hirano, A.; Tanaka, T.; Urabe, Y.; Kataura, H. pH- and Solute-Dependent Adsorption of Single-Wall Carbon Nanotubes onto Hydrogels: Mechanistic Insights into the Metal/Semiconductor Separation. *ACS Nano* **2013**, *7*, 10285–10295.
30. Flavel, B. S.; Kappes, M. M.; Krupke, R.; Hennrich, F. Separation of Single-Walled Carbon Nanotubes by 1-Dodecanol-Mediated Size-Exclusion Chromatography. *ACS Nano* **2013**, *7*, 3557–3564.
31. Blanch, A. J.; Quinton, J. S.; Shapter, J. G. The Role of Sodium Dodecyl Sulfate Concentration in the Separation of Carbon Nanotubes Using Gel Chromatography. *Carbon* **2013**, *60*, 471–480.
32. Bales, B. L. A Definition of the Degree of Ionization of a Micelle Based on Its Aggregation Number. *J. Phys. Chem. B* **2001**, *105*, 6798–6804.
33. Silvera-Batista, C. A.; Scott, D. C.; McLeod, S. M.; Ziegler, K. J. A Mechanistic Study of the Selective Retention of SDS-Suspended Single-Wall Carbon Nanotubes on Agarose Gels. *J. Phys. Chem. C* **2011**, *115*, 9361–9369.

34. Hirano, A.; Tanaka, T.; Kataura, H. Thermodynamic Determination of the Metal/Semiconductor Separation of Carbon Nanotubes Using Hydrogels. *ACS Nano* **2012**, *6*, 10195–10205.

35. Tulevski, G. S.; Franklin, A. D.; Afzali, A. High Purity Isolation and Quantification of Semiconducting Carbon Nanotubes *via* Column Chromatography. *ACS Nano* **2013**, *7*, 2971–2976.

36. Tanaka, T.; Urabe, Y.; Nishide, D.; Kataura, H. Discovery of Surfactants for Metal/Semiconductor Separation of Single-Wall Carbon Nanotubes *via* High-Throughput Screening. *J. Am. Chem. Soc.* **2011**, *133*, 17610–17613.

37. Duque, J. G.; Densmore, C. G.; Doorn, S. K. Saturation of Surfactant Structure at the Single-Walled Carbon Nanotube Surface. *J. Am. Chem. Soc.* **2010**, *132*, 16165–16175.

38. Duque, J. G.; Oudjedi, L.; Crochet, J. J.; Tretiak, S.; Lounis, B.; Doorn, S. K.; Cognet, L. Mechanism of Electrolyte-Induced Brightening in Single-Wall Carbon Nanotubes. *J. Am. Chem. Soc.* **2013**, *135*, 3379–3382.

39. Niyogi, S.; Densmore, C. G.; Doorn, S. K. Electrolyte Tuning of Surfactant Interfacial Behavior for Enhanced Density-Based Separations of Single-Walled Carbon Nanotubes. *J. Am. Chem. Soc.* **2008**, *131*, 1144–1153.

40. Yurekli, K.; Mitchell, C. A.; Krishnamoorti, R. Small-Angle Neutron Scattering from Surfactant-Assisted Aqueous Dispersions of Carbon Nanotubes. *J. Am. Chem. Soc.* **2004**, *126*, 9902–9903.

41. Tummala, N. R.; Striolo, A. SDS Surfactants on Carbon Nanotubes: Aggregate Morphology. *ACS Nano* **2009**, *3*, 595–602.

42. Xu, Z.; Yang, X.; Yang, Z. A Molecular Simulation Probing of Structure and Interaction for Supramolecular Sodium Dodecyl Sulfate/Single-Wall Carbon Nanotube Assemblies. *Nano Lett.* **2010**, *10*, 985–991.

43. White, B.; Banerjee, S.; O'Brien, S.; Turro, N. J.; Herman, I. P. Zeta-Potential Measurements of Surfactant-Wrapped Individual Single-Walled Carbon Nanotubes. *J. Phys. Chem. C* **2007**, *111*, 13684–13690.

44. Rajter, R. F.; Podgornik, R.; Parsegian, V. A.; French, R. H.; Ching, W. Y. Van Der Waals-London Dispersion Interactions for Optically Anisotropic Cylinders: Metallic and Semiconducting Single-Wall Carbon Nanotubes. *Phys. Rev. B* **2007**, *76*, 045417.

45. Hobbie, E. K.; Ihle, T.; Harris, J. M.; Semler, M. R. Empirical Evaluation of Attractive Van Der Waals Potentials for Type-Purified Single-Walled Warbon Nanotubes. *Phys. Rev. B* **2012**, *85*, 245439.

46. Ohshima, H. Electrostatic Interaction between a Cylinder and a Planar Surface. *Colloid Polym. Sci.* **1999**, *277*, 563−569.

47. LeMieux, M. C.; Roberts, M.; Barman, S.; Jin, Y. W.; Kim, J. M.; Bao, Z. N. Self-Sorted, Aligned Nanotube Networks for Thin-Film Transistors. *Science* **2008**, *321*, 101–104.

48. Jones, J. E. On the Determination of Molecular Gields - II From the Equation of State of a Gas. *Proc. R. Soc. London Ser. A* **1924**, *106*, 463−477.

49. Jeng, E. S.; Shih, C.-J.; Barone, P. W.; Jones, N.; Baik, J. H.; Abrahamson, J. T.; Strano, M. S. A Compositional Window of Kinetic Stability for Amphiphilic Polymers and Colloidal Nanorods. *J. Phys. Chem. C* **2011**, *115*, 7164–7170.

50. Fuchs, N. Theory of Coagulation. *Z. Phys.* **1934**, *171*, 199–208.

51. Bloomfield, V.; Dalton, W. O.; Vanholde, K. E. Frictional Coefficients of Multisurbunit Structures 0.1. Theory. *Biopolymers* **1967**, *5*, 135–148.

52. Incropera, F. P.; DeWitt, D. P. *Fundamentals of Heat and Mass Transfer*, 5th ed.; John Wiley & Sons: Hoboken, NJ, 2002.

53. Lucas, A.; Zakri, C. c.; Maugey, M.; Pasquali, M.; Schoot, P. v. d.; Poulin, P. Kinetics of Nanotube and Microfiber Scission under Sonication. *J. Phys. Chem. C* **2009**, *113*, 20599–20605.

54. Nair, N.; Kim, W. J.; Braatz, R. D.; Strano, M. S. Dynamics of Surfactant-Suspended Single-Walled Carbon Nanotubes in a Centrifugal Field. *Langmuir* **2008**, *24*, 1790–1795.

55. Ohshima, H. Electrostatic Interaction between Two Parallel Cylinders. *Colloid Polym. Sci.* **1996**, *274*, 1176–1182.

56. Heller, D. A.; Barone, P. W.; Swanson, J. P.; Mayrhofer, R. M.; Strano, M. S. Using Raman Spectroscopy to Elucidate the Aggregation State of Single-Walled Carbon Nanotubes. *J. Phys. Chem. B* **2004**, *108*, 6905–6909.

57. Huang, Y. Y.; Terentjev, E. M. Dispersion of Carbon Nanotubes: Mixing, Sonication, Stabilization, and Composite Properties. *Polymers* **2012**, *4*, 275–295.

58. Naumov, A. V.; Ghosh, S.; Tsyboulski, D. A.; Bachilo, S. M.; Weisman, R. B. Analyzing Absorption Backgrounds in Single-Walled Carbon Nanotube Spectra. *ACS Nano* **2011**, *5*, 1639−1648.

59. Schoppler, F.; Mann, C.; Hain, T. C.; Neubauer, F. M.; Privitera, G.; Bonaccorso, F.; Chu, D. P.; Ferrari, A. C.; Hertel, T. Molar Extinction Coefficient of Single-Wall Carbon Nanotubes. *J. Phys. Chem. C* **2011**, *115*, 14682–14686.